Combustion and Flame 161 (2014) 1507–1515

Contents lists available at ScienceDirect

Combustion and Flame

journal homepage: www.elsevier.com/locate/combustflame

Entropy production analysis for mechanism reduction

Mahdi Kooshkbaghi, Christos E. Frouzakis *, Konstantinos Boulouchos, Ilya V. Karlin

Aerothermochemistry and Combustion Systems Laboratory, Swiss Federal Institute of Technology, Zurich CH-8092, Switzerland

ARTICLE INFO

Article history:
Received 28 August 2013
Received in revised form 28 October 2013
Accepted 17 December 2013
Available online 11 January 2014

Keywords:
Skeletal mechanism
Mechanism reduction
Entropy production

ABSTRACT

A systematic approach based on the relative contribution of each elementary reaction to the total entropy production is developed for eliminating species from detailed reaction mechanisms in order to generate skeletal schemes. The approach is applied to a database of solutions for homogeneous constant pressure auto-ignition of *n*-heptane to construct two skeletal schemes for different threshold values defining the important reactions contributing to the total entropy production. The accuracy of the skeletal mechanisms is evaluated in spatially homogeneous systems for ignition delay time, a single-zone engine model, and a perfectly stirred reactor in a wide range of thermodynamic conditions. High accuracy is also demonstrated for the speed and structure of spatially-varying premixed laminar flames.

1. Introduction

Detailed reaction mechanisms of practical fuels provide accurate predictions of the combustion process over wide ranges of temperature, pressure and compositions. For large hydrocarbons, the detailed description typically includes hundreds of species participating in thousands of elementary chemical reactions. Incorporating such a detailed reaction mechanism into multidimensional simulations is practically impossible. In addition to the large number of variables, discretization of the spatial terms and the disparate time scales result in excessively large systems of stiff nonlinear ordinary differential equations (ODEs). Reactive flow simulations using detailed reaction mechanisms have demonstrated that a significant part of the total computational cost is spent in solving the stiff ODEs for species with negligible concentration [1]. Different methods for reducing the computational cost have been proposed in the literature. A brief overview of the reduction approaches is presented below while more detailed descriptions can be found in recent reviews [2–4].

The solution storage/retrieval approaches are based on the tabulation of frequently visited states during the simulation. The quantities are stored only for the accessible regions of the chemically admissible space. The in situ Adaptive Tabulation (ISAT) [5], Piecewise Reusable Implementation (PRISM) [6] and orthogonal polynomials storage method [7] belong to this category.

Other methods are based on the decomposition of motion in phase space into fast and slow. Various methods are used to find an accurate description of the slow subsystem which dominates the long-time behavior. The group of species associated with the fast timescales can then be represented (usually implicitly) as functions of the species associated with the slow subspace. The Quasi Steady State Approximation (QSSA) and the Partial Equilibrium Assumption (PEA) are two well known classical methods for this purpose [8]. The Computational Singular Perturbation (CSP) [9], Intrinsic Low Dimensional Manifold (ILDM) [10] and Method of Invariant Manifold (MIM) [11] were proposed based on the dynamical systems point of view for model reduction which stems from the attractive low dimensional Slow Invariant Manifold (SIM) concept. In the resulting reduced schemes the differential equations for the fast-evolving species are replaced by systems of algebraic equations or tables, and the reduced system is significantly less stiff than the original set of equations. Although simplified models obtained by reduction techniques can reduce the computational cost, retaining maximum fidelity to the underlying non-linear dynamical system is not possible when the fast and slow time scales are not sufficiently decoupled. For example, in the case of oscillatory dynamics, reduced model based on QSSA have been shown to miss the bifurcation type (sub- vs. supercritical) and significantly modify the amplitude of the limit cycle [12]. In addition, there can still be a significant computational cost associated with the solution of the typically non-linear system of algebraic equations and/or the retrieval of information from the tables. For large reaction mechanisms, unimportant species and reactions should therefore be eliminated prior to using reduction methods based on time scale analysis [13].

The third group of methods introduces skeletal reduction techniques. The skeletal mechanism can be generated by eliminating reactions and/or species [1,14]. Elimination of unimportant reactions can be performed using, for example, sensitivity analysis

* Corresponding author. Address: Aerothermochemistry and Combustion Systems Laboratory, Swiss Federal Institute of Technology (ETH), Sonnegstrasse 3, Zurich CH-8092, Switzerland.
E-mail address: frouzakis@lav.mavt.ethz.ch (C.E. Frouzakis).

0010-2180/$ - see front matter © 2013 The Combustion Institute. Published by Elsevier Inc. All rights reserved.
http://dx.doi.org/10.1016/j.combustflame.2013.12.016

[15], the importance index of CSP [16], Principal Component Analysis (PCA) [17] or optimization-based methods [18,19]. Due to their nonlinear coupling, the direct elimination of species is more challenging. CSP [16,20–23], Directed Relation Graph (DRG) [13,24–27], DRG with Error Propagation (DRGEP) [28,29], DRG-Aided Sensitivity Analysis (DRGASA) [30,31], Transport Flux-Based DRG (TFBDRG) [32], Path Flux Analysis (PFA) [33,34] and necessity analysis [35] have been employed for species elimination. In addition, species with similar thermal and transport properties and diffusivities can be lumped together to further reduce the size of the skeletal mechanism [36–38]. Selecting important species during the simulation (on the fly model reduction) is also possible as proposed for example by the Dynamic Adaptive Chemistry (DAC) reduction method [39,40]. The aforementioned methods can be combined with storage/retrieval approaches [41].

For large mechanisms, approaches which select species based on the slow/fast decomposition bear heavy computational cost because of the timescale analysis of the Jacobian matrix of the associated large system of ODEs. On the other hand, QSSA, PEA and sensitivity analysis require additionally mechanism-dependent knowledge. The methods which are based on the graph structure relation between species sometimes need a careful a priori choice of the group of target species [39].

In addition to timescale analysis, thermodynamic properties of the system have been used to determine low dimensional manifolds. The Rate Controlled Constrained Equilibrium (RCCE) is based on the second law and assumes that the system state evolves through a sequence of constrained-equilibrium (or quasi-equilibrium) states, which are obtained by maximizing entropy subject to a small number of constraints imposed by certain classes of rate-controlling reactions [42,43]. It has been shown that in some cases the RCCE manifold results in large errors in the evolution of the reduced system in comparison with the detailed description, particularly for species with small concentration [44]. Entropy production has also been used for the slow/fast timescale decomposition of dynamics and construction of the SIM. In particular, the closest to the equilibrium trajectory known as Minimal Entropy Production Trajectory (MEPT) was considered as the SIM [45]. As it was shown in [46], however, low dimensional manifolds resulting from methods employing classical thermodynamic functions can only approximate the actual SIM. Nevertheless, in the scope of chemical kinetics, important reactions in different regions of composition space can be characterized by the local entropy production [47,48].

In the present study, the relative contribution of elementary reactions in the total entropy production is proposed as a criterion for the construction of accurate skeletal reaction mechanisms. The important reactions are identified based on their relative contribution to the total entropy production being larger than a user-specified threshold. This criterion leads to a procedure that is easy to implement without any prior knowledge about the detailed mechanism. Skeletal mechanisms of different sizes can be obtained by choosing the threshold based on desired deviation from the results obtained with the detailed reaction mechanism.

A significant reduction in the number of species as well as the stiffness of the system is reported here for the case of a detailed mechanism for *n*-heptane. The skeletal mechanisms are shown to provide very accurate results at a fraction of the computational cost in comparison to the detailed mechanism for various cases over a wide range of thermodynamic conditions. Compared to the other methods such as [13,23], the same level of reduction can be achieved with the much simpler entropy production analysis.

The paper is organized as follows. In Section 2, the basic notion of the entropy production for chemical kinetics is briefly reviewed. The features and algorithm of the method for skeletal mechanism reduction are presented in Section 3. In Section 4, the algorithm is applied on a database generated using a detailed *n*-heptane mechanism and two skeletal mechanisms are validated in terms of ignition delay time, in a homogeneous engine model, a perfectly stirred reactor and laminar premixed flame. Conclusions are drawn in Section 5. Finally, instructions on the numerical procedure of the entropy production analysis are presented in the appendix.

2. Entropy production for chemical kinetics

For the sake of completeness, the notion of the entropy production is briefly reviewed in this section following the formalism of [49]. For a detailed discussion of the entropy and entropy production concepts for chemical kinetics and other systems the reader is also referred to [50,43].

The changes in the entropy for a system at local equilibrium is expressed as

$$dS = d^{ex}S + d^{in}S \tag{1}$$

where superscripts 'in' and 'ex' denote the change of the system entropy due to interactions inside the domain and with its environment [49].

Chemical reactions describe the change in the number of moles of the n_s reactants represented by the vector $\underline{N} = (N_1, \ldots, N_{n_s})^T$. The change in the chemical composition of the species is the result of n_r reversible reactions,

$$\sum_{i=1}^{n_s} \nu'_{ik} N_i \rightleftharpoons \sum_{i=1}^{n_s} \nu''_{ik} N_i, \quad k = 1, \ldots, n_r \tag{2}$$

where, the ν'_{ik} and ν''_{ik} are the stoichiometric coefficients of the ith species in the kth reaction for the reactants and products, respectively. The rate of progress q_k of the kth reaction is given by the difference of the forward and reverse reaction rates

$$q_k = q_{f_k} - q_{r_k} = k_{f_k} \prod_{i=1}^{n_s} [N_i]^{\nu'_{ik}} - k_{r_k} \prod_{i=1}^{n_s} [N_i]^{\nu''_{ik}}, \quad k = 1, \ldots, n_r \tag{3}$$

where $[N_i]$ denotes the molar concentration of the ith species and k_{f_k} and k_{r_k} are the forward and reverse rate constants of the kth reaction having the Arrhenius form

$$k_{f_k} = A_k T^{\beta_k} \exp\left(\frac{-E_k}{R_c T}\right) \tag{4}$$

with A_k, β_k, E_k and R_c being the pre-exponential factor, temperature exponent, activation energy and ideal gas constant, respectively. The reverse and forward rate constants are related via the equilibrium constant, K_{C_k}

$$k_{r_k} = \frac{k_{f_k}}{K_{C_k}} \tag{5}$$

where

$$K_{C_k} = exp\left(\frac{\Delta S_k^0}{R} - \frac{\Delta H_k^0}{R_c T}\right) \left(\frac{p_{atm}}{R_c T}\right)^{\sum_{i=1}^{ns} (\nu''_{ik} - \nu'_{ik})} \tag{6}$$

$p_{atm} = 1$ bar, and $\Delta S_k^0, \Delta H_k^0$ are the entropy and enthalpy changes for reaction k.

For a closed homogeneous system, the rate of change of the concentration of the ith species is given by

$$\frac{d[N_i]}{dt} = [\dot{N}_i] = \sum_{k=1}^{r} (\nu''_{ik} - \nu'_{ik}) q_k, \quad i = 1, \ldots, n_s \tag{7}$$

Using the reactor volume V, we can rewrite (7) in vector form as

$$\frac{d\underline{N}}{dt} = V[\dot{\underline{N}}] = \underline{f}(\underline{N}) \tag{8}$$

The change of the ith species in the kth reaction is related to the change in the extent of the reaction, ξ_k, as

$$\frac{dN_i}{\nu''_{ik}-\nu'_{ik}} = d\xi_k, \quad i = 1,\ldots,n_s \quad k = 1,\ldots,n_r \tag{9}$$

where

$$\frac{d\xi_k}{dt} = V(q_{f_k} - q_{r_k}) \tag{10}$$

The fundamental equation of chemical thermodynamics in terms of the internal energy reads

$$dU = TdS - pdV + \sum_{i=1}^{n_s}\mu_i dN_i \tag{11}$$

μ_i being the chemical potential of the ith species

$$\mu_i = \left(\frac{\partial U}{\partial N_i}\right)_{S,V,N_{l\neq i}}, \quad i = 1,\ldots,n_s \tag{12}$$

The de Donder affinity ([51]) of reaction k is defined as

$$\alpha_k = -\Sigma_{i=1}^{n_s}(\nu''_{ik}-\nu'_{ik})\mu_i, \quad k = 1,\ldots,n_r \tag{13}$$

In the absence of deviations from the principle of detailed balance ([43]), α_k becomes

$$\alpha_k = R_c T \ln\left(\frac{q_{f_k}}{q_{r_k}}\right) \tag{14}$$

The change in the number of moles of each species can be decomposed into the change due to irreversible chemical reactions, $d^{in}N_i$, and exchange of matter with the system exterior, $d^{ex}N_i$ [52].

$$dN_i = d^{in}N_i + d^{ex}N_i, \quad i = 1,\ldots,n_s \tag{15}$$

For open systems, the entropy exchange with the exterior is of the form

$$d^{ex}S = \frac{dU + pdV}{T} - \frac{\sum_{i=1}^{n_s}\mu_i d^{ex}N_i}{T} \tag{16}$$

while the entropy change due to the change in mole numbers with respect to chemical reactions reads

$$d^{in}S = -\frac{\sum_{i=1}^{n_s}\mu_i d^{in}N_i}{T} \tag{17}$$

For a closed system, $d^{ex}N = 0$ so that $dN = d^{in}N$ and the entropy production due to a chemical reaction is,

$$\frac{d^{in}S}{dt} = -\frac{1}{T}\sum_{i=1}^{n_s}\mu_i\frac{dN_i}{dt} \tag{18}$$

where $\frac{dN_i}{dt}$ can be written in terms of the extent of reactions using (9),

$$\frac{dN_i}{dt} = \sum_{k=1}^{n_r}(\nu''_{ik}-\nu'_{ik})\frac{d\xi_k}{dt} \tag{19}$$

Hence, entropy production is

$$\frac{d^{in}S}{dt} = -\frac{1}{T}\sum_{i=1}^{n_s}\mu_i\sum_{k=1}^{n_r}\frac{d\xi_k}{dt}(\nu''_{ik}-\nu'_{ik}) \tag{20}$$

which, by using the affinity definition can be written as (13),

$$\frac{d^{in}S}{dt} = \frac{1}{T}\sum_{k=1}^{n_r}\alpha_k\frac{d\xi_k}{dt} \tag{21}$$

Using (10) and (14), the total entropy production per unit volume, a positive semi-definite function which vanishes at equilibrium, becomes

$$\frac{d^{in}S}{dt} = R_c\sum_{k=1}^{n_r}(q_{f_k}-q_{r_k})\ln\left(\frac{q_{f_k}}{q_{r_k}}\right) \geqslant 0 \tag{22}$$

Finally, the relative contribution of each reaction to the total entropy production at time t, $r_k(t)$ is defined as

$$r_k(t) = \left(\frac{d^{in}S}{dt}\right)^{-1}\left[R_c(q_{f_k}-q_{r_k})\ln\left(\frac{q_{f_k}}{q_{r_k}}\right)\right] \tag{23}$$

From Eq. (23) it is clear that for reactions at equilibrium $r_k(t) = 0$.

3. Skeletal reduction using entropy production analysis

In this paper, the relative contribution of each reaction to the total entropy production is considered as a measure of its importance. The steps for finding the subset of the reactions that at the time t of interest forms the skeletal mechanism are summarized below:

1. Identify the *most-contributing reactions*, i.e. the reactions which contribute at least ϵ to the total entropy production

$$r_k(t) \geqslant \epsilon \tag{24}$$

2. Identify the *important species*, i.e. the species participating in the most-contributing reactions.
3. Generate the skeletal mechanism at time t by eliminating the non-important species from the detailed description using a slightly modified version of MECHMOD 3.42 [53].

Note that each important species participate in at least one most-contributing reaction. Following step 3, the skeletal mechanism contains not only the most contributing reactions, but all elementary reactions which include important species on both sides as well. Further reduction of the number of reactions (with the same number of species) would necessitate further analysis such as reaction path or atomic flux [33] to quantify the contribution of each reaction in the total production or consumption rate of the species.

The local analysis of the entropy production can be applied at different time instants during the temporal evolution of the system state. The analysis can be extended to a database of trajectories computed for a range of pressures, initial temperatures and compositions to construct a global skeletal mechanism. The most-contributing reactions are considered as the reactions which at least once have a significant contribution in the entropy production of the whole database, and the final skeletal mechanism is valid within the range of conditions represented by the sample data. The algorithm of the present simple procedure is provided in appendix A using CHEMKIN's notation [54].

Finally, it should be pointed out that the term q_{f_k}/q_{r_k} in the logarithm of (22) must be strictly positive. This condition is violated in two cases:

(a) irreversible reactions where the backward reaction rate is zero ($q_{r_k} = 0$);
(b) when low negative concentrations result from numerical issues ($q_{f_k} < 0$ and/or $q_{r_k} < 0$).

In case (a) the q_{r_k}, and in the case (b) q_{f_k} and/or q_{r_k} should be set to be a small (chemically insignificant) positive number (e.g. 10^{-50} in our study). The problem of partially irreversible limit in chemical thermodynamics is addressed in the recent study [55].

4. Skeletal mechanism for *n*-heptane

The kinetics of *n*-heptane is of interest not only as its own right as a representative of the kinetics of higher hydrocarbons displaying the Negative Temperature Coefficient (NTC) regime and multi-stage ignition, but also as one of the components of the Primary Reference Fuel (PRF) used for octane rating for internal combustion engines [56].

The comprehensive mechanism for *n*-heptane consisting of 561 species and 2539 reactions (LLNL mechanism version 2, [57]) was developed to study oxidation for pressures in the range $1 \leqslant p \leqslant 42$ atm, initial temperatures between 550 and 1700 K, equivalence ratio ϕ from 0.3 to 1.5, and nitrogen-argon dilution from 70% to 99% [58]. The detailed mechanism which will be referred to as D561 below has been used for the development of reduced schemes by various approaches [13,23,26,38,59].

The local entropy production analysis is performed at the four time instants during the isobaric and isenthalpic auto-ignition of a stoichiometric mixture at initial temperature and pressure $T_0 = 650$ K, $p = 1$ atm marked in Fig. 1 in order to identify the reactions contributing at least $\epsilon = 0.05$ to the total entropy production.

The analysis reveals that initially ($t = 0$ s) the important reactions are those of oxygen attacking the fuel to produce HO_2 and the heptyl radical isomers

$$nC_7H_{16} + O_2 \rightleftharpoons C_7H^-_{153} + HO_2$$
$$nC_7H_{16} + O_2 \rightleftharpoons C_7H^-_{152} + HO_2$$
$$nC_7H_{16} + O_2 \rightleftharpoons C_7H^-_{154} + HO_2$$
$$nC_7H_{16} + O_2 \rightleftharpoons C_7H^-_{151} + HO_2$$

During the first pre-ignition period ($t = 0.02$ and 0.056 s), reactions with OH radicals abstracting H from the fuel

$$nC_7H_{16} + OH \rightleftharpoons C_7H^-_{152} + H_2O$$
$$nC_7H_{16} + OH \rightleftharpoons C_7H^-_{153} + H_2O$$

thermal decomposition

$$C_7H_{14}OOH^-_{25} \rightleftharpoons C_7H_{14}O^-_{25} + OH$$
$$C_7H_{14}OOH^-_{36} \rightleftharpoons C_7H_{14}O^-_{25} + OH$$
$$C_7H_{14}OOH^-_{14} \rightleftharpoons C_7H_{14}O^-_{14} + OH$$

and ketohydroperoxides decomposition

$$nC_7ket_{24} \rightarrow nC_3H_7CHO + CH_3COCH_2 + OH$$
$$nC_7ket_{35} \rightarrow C_2H_5CHO + C_2H_5COCH_2 + OH$$

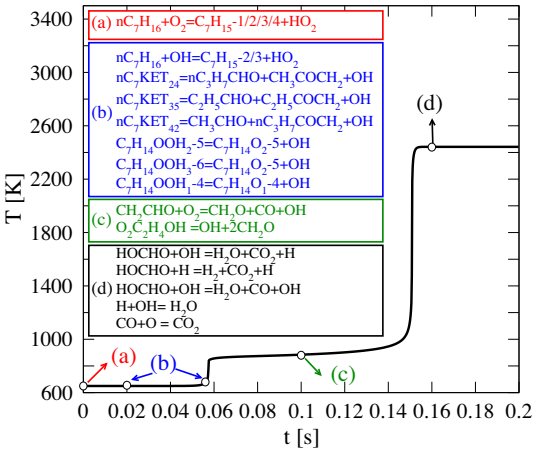

Fig. 1. Temporal evolution of temperature computed using the detailed mechanism and the major elementary reactions at different times ($\phi = 1, p = 1$ atm, $T_0 = 650$ K).

contribute significantly to entropy production. The most-contributing reactions during the period before the second ignition ($t = 0.1$ s) are the ones producing formaldehyde (CH_2O) and carbon monoxide (CO)

$$CH_2CHO + O_2 \rightarrow CH_2O + CO + OH$$
$$O_2C_2H_4OH \rightarrow OH + 2CH_2O$$

The analysis of post-ignition at $t = 0.16$ s shows that the most-contributing reactions are those producing the main products (CO_2, CO and H_2O)

$$HOCHO + OH \rightarrow H_2O + CO_2 + H$$
$$HOCHO + H \rightarrow H_2 + CO_2 + H$$
$$HOCHO + OH \rightarrow H_2O + CO + OH$$

The distribution of entropy production among reactions for different times is summarized in Fig. 2.

It should be noted that the important reactions, products and oxidation path found here on the basis of the entropy production analysis are in agreement with the results of the kinetic description of *n*-heptane oxidation [58] and the CSP analysis [23].

Entropy production analysis was then performed on a solution database for auto-ignition in the range of pressures 1, 5, 10, 20 atm, initial temperatures $650 \leqslant T_0 \leqslant 1400$ K resolved with a step of 50 K, equivalence ratios $\phi = 0.5, 0.8, 1.0, 1.2, 1.5$ and different threshold values ϵ. The dependence of the error in the ignition delay time and the number of species in the skeletal mechanism on the threshold are plotted in Fig. 3 for $p = 1$ atm, $T_0 = 650$ K and $\phi = 1.0$. The non-monotonicity of the error curve has also been observed in other species elimination techniques based on analysis of reactive states [34,60].

Two skeletal mechanisms with 161 species in 688 reactions and 203 species in 879 reactions obtained with $\epsilon = 0.006$ and 0.002 and henceforth referred to as R161 and R203, respectively, were selected for validation. It should be noted that smaller schemes can be readily constructed, albeit at the cost of narrower range of applicability and/or lower accuracy. Similar species can also be lumped together as proposed in [38,26] to further reduce the size of the mechanism.

The size of the mechanism obtained by the entropy production analysis is comparable with other reduction approaches. With the same quality of reduction, a skeletal mechanism including 188 species and 842 reactions was obtained by DRG [13], and 177 species and 768 reactions or 185 species and 786 reactions by CSP [23].

4.1. Auto-ignition of homogeneous mixture

Ignition delay times in the constant pressure and enthalpy reactor computed using the skeletal and detailed mechanisms are compared in Fig. 4. Both skeletal mechanisms reproduce the ignition delay well over a wide range of pressures, equivalence ratios and temperatures including the NTC region. As expected, better agreement is obtained at high pressures and temperatures and the error for R161 is higher than that of R203.

Species elimination with the help of entropy production leads not only to an ODE system of reduced dimensionality but also with lower stiffness. The evolution of the fastest timescale, τ_{fast}, defined by the inverse of the most negative eigenvalue of the Jacobian matrix for the D561, R203 and R161 schemes is plotted in Fig. 5, together with the time history of temperature. The fast timescale is monotonically decreasing towards equilibrium, while there are sharp drops during the two ignition stages. The difference between the timescales of the detailed and skeletal mechanisms are several orders of magnitude which in combination with the reduced number of variables results in a significant reduction in computational time even for homogeneous autoignition computations. CPU times

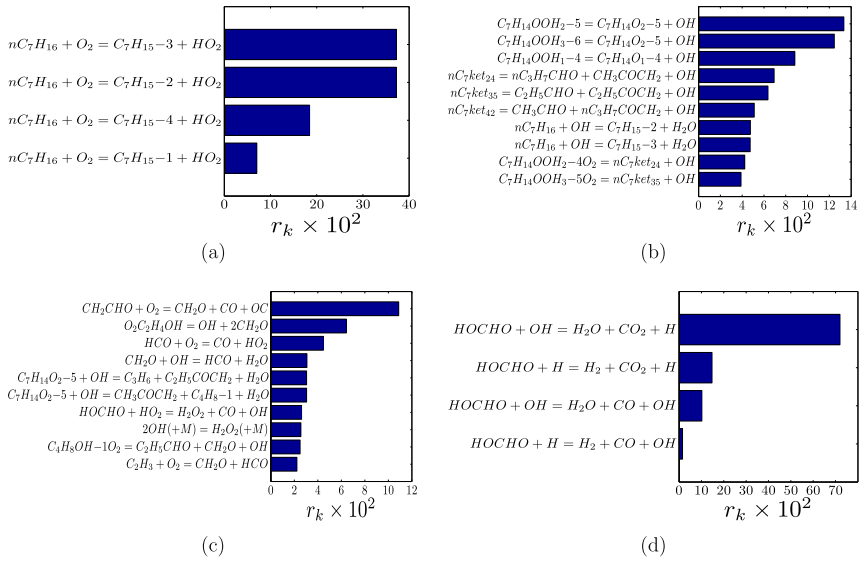

Fig. 2. Entropy production contributions of elementary reactions using the detailed mechanism ($T_0 = 650$ K,$p = 1$ atm and $\phi = 1$); (a) $t = 0$ s, (b) $t = 0.03$ s, (c) $t = 0.1$ s, (d) $t = 0.16$ s.

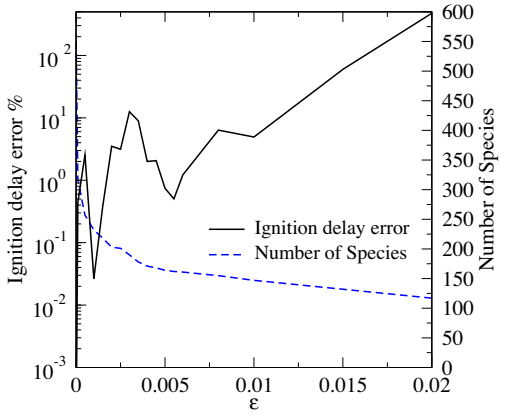

Fig. 3. Number of species in the skeletal mechanism and relative error in the ignition delay time as a function of the threshold ($\phi = 1.0, p = 1$ atm, $T_0 = 650$ K).

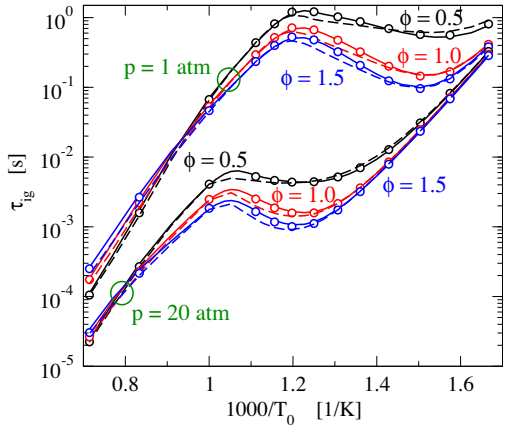

Fig. 4. Ignition delay times computed with the different reaction mechanisms (D561: solid line, R203: circles, R161: dashed line).

for the calculation of 1 s of the ignition process for three initial temperature are summarized in Table 1 using the stiff ODE integrator DVODE [61]; the speed up for R203 and R161 compared with D561 is around 10.3 and 16, respectively. Similar order of timescales for *n*-heptane was also reported in [59]. It should be noted that the unrealistically fast time scales of the order of 10^{-15} s may well be an artifact of the way the detailed mechanisms for such complex fuels are generated (automatic generation based on the so-called reaction classes [58]).

The corresponding curves of the total entropy production per volume are compared in Fig. 6. The peaks in the entropy production correspond to the ignition stages; the entropy production

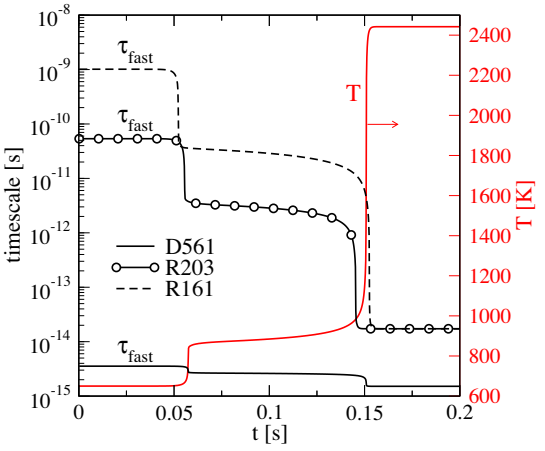

Fig. 5. Temporal evolution of the temperature and the fastest timescale of the homogeneous autoigintion system for the skeletal (R203: circles with solid line, R161: dashed line) and detailed (solid line) mechanism ($\phi = 1.0, p = 1$ atm, $T_0 = 650$ K).

Table 1
CPU times (seconds) for the integration of the isobaric and isenthalpic reactor for 1 s ($\phi = 1, p = 1$ atm).

	$T_0 = 600$ K	$T_0 = 650$ K	$T_0 = 700$ K	$T_0 = 750$ K
D561	111.9	97.5	98.7	88.5
R203	10.8	10.0	9.1	8.5
R161	6.6	6.5	6.0	5.7

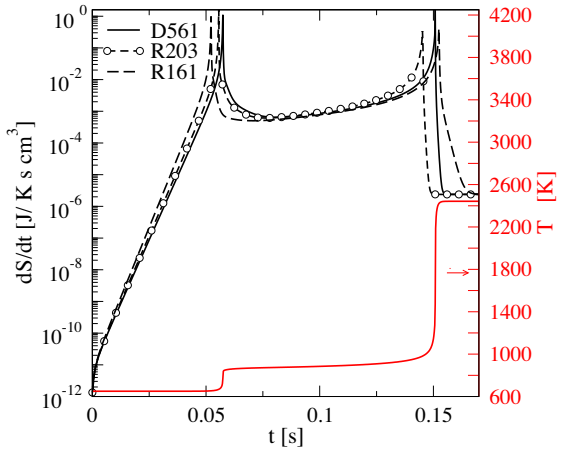

Fig. 6. Time history of the entropy production (D561: solid line, R203: circles, R161: dashed line) for $\phi = 1.0, p = 1$ atm, $T_0 = 650$ K.

history of the detailed solution is well reproduced by both R203 and R161. At equilibrium the entropy reaches its maximum and dS/dt tends to zero (Fig. 6) albeit at a decreasing rate (Eq. (22)). In the presence of irreversible reactions and negative concentration resulting from numerical issues (as is the case here), the value of dS/dt at long times is affected by the value chosen for the regularization of zero or negative reaction rates (see Section 3).

4.2. Perfectly stirred reactor

The skeletal mechanisms were further validated in a Perfectly Stirred Reactor (PSR) simulation. The stoichiometric mixture of *n*-heptane with the inlet temperature, $T_0 = 650$ K is considered at different pressures and for an extended range of residence times. The reactor temperature and OH mass fraction as a function of the residence time are plotted in Fig. 7(a) and (b), respectively. The profiles calculated with the R161 and R203 agree very well with those of the detailed mechanism for all residence times and pressures. In addition, the turning points are also accurately captured with the skeletal mechanisms, proving that the complex dynamics of *n*-heptane is reproduced by the skeletal mechanisms over a wide range of conditions.

4.3. Single-zone engine model

In the absence of spatial inhomogeneities, a single-zone engine model can be used for a reciprocating engine with adiabatic boundary conditions [62]. The governing equations for the temporal evolution of the species mass fractions, Y_i, temperature and pressure read

$$\begin{aligned} \frac{dY_i}{dt} &= \frac{\dot{\omega}_i W_i}{\rho} \\ \frac{dT}{dt} &= \frac{1}{c_v}\left(-p\frac{d(1/\rho)}{dt} - \frac{\sum_i e_i \dot{\omega}_i W_i)}{\rho}\right) \\ p &= \frac{R_c T \rho}{\overline{W}} \end{aligned} \tag{25}$$

where $\rho, \overline{W}$ and c_v are the density, mean molecular weight and mean specific heat at constant volume of the mixture, and R_c the ideal gas constant. Thermodynamic properties, production rates, $\dot{\omega}_i$, and specific internal energy, e_i, of the ith species are computed, using the CHEMKIN library [54]. The change of density in time is the function of the cylinder volume and the total mass of the reacting

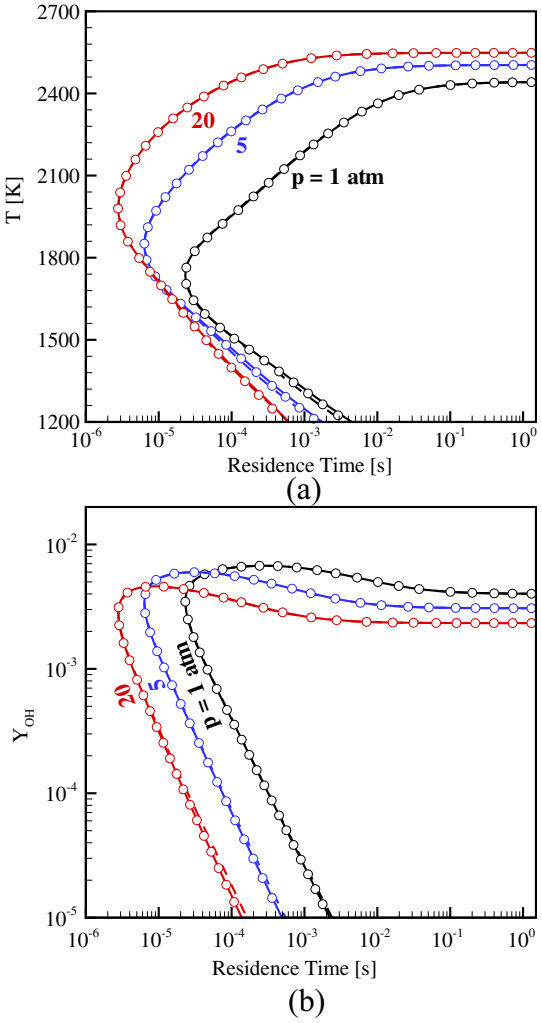

Fig. 7. The dependence of the reactor temperature (a) and OH mass fraction (b) on pressure and residence time in a PSR ($\phi = 1$, inlet mixture temperature $T_{in} = 650$ K) (D561: solid line, R203: circles, R161: dashed line).

mixture. The change of volume, $V(t)$, can be related to the crank angle, θ [62]

$$\frac{V(t)}{V_c} = 1 + \frac{1}{2}(r_c - 1)f(\theta) \tag{26}$$

with

$$f(\theta) = l/a + 1 - cos(\theta(t)) - \sqrt{(l/a)^2 - sin(\theta(t))} \tag{27}$$

where V_c is the clearance volume (minimum cylinder volume), l/a is the ratio of the connecting rod length to the crank radius and r_c is the compression ratio. The simulation are carried out for an engine with $V_c = 125$ ml, $l/a = 3$ and $r_c = 10$. The initial temperature and pressure for the lean mixture ($\phi = 0.8$) at -40° ATDC (after top dead center) are 750 K and 5 atm, respectively. The pressure and temperature traces for 700 rpm are compared in Fig. 8(a) and (b): the differences between the results are of the same order as for the ignition delay. The profiles for selected species in Fig. 8(c) and (d) shows excellent agreement for the major species and radicals even at very low concentrations. It should be noted that the skeletal mechanisms are constructed using data in the range $1 \leqslant p \leqslant 20$ atm, but in this case the pressure is increasing up to

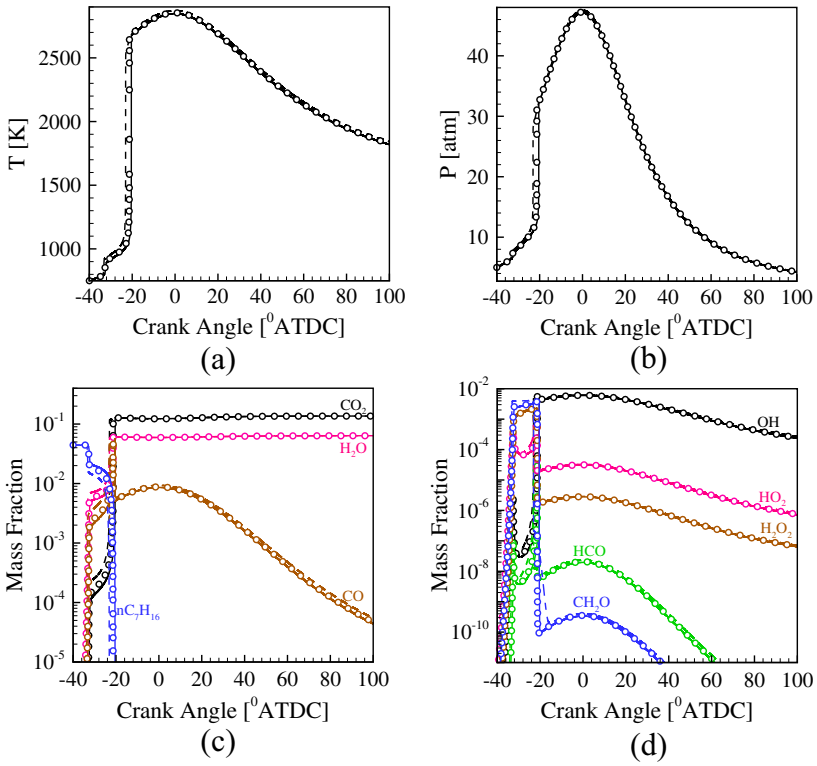

Fig. 8. Time history of (a) temperature, (b) pressure, and (c–d) selected species concentration profiles for the single-zone engine model. The lean fresh mixture ($\phi = 0.8$) is injected at -40^0 ATDC with $p_0 = 5$ atm and $T_0 = 750$ K (D561: solid line, R203: circles, R161: dashed line).

47 atm. As mentioned in Section 4.1, the agreement between the skeletal and detailed models are generally better at high pressures.

4.4. Premixed flame

The accuracy of the skeletal mechanisms generated using data for a homogeneous system were finally validated in an atmospheric 1-D laminar premixed flame with an unburned mixture temperature $T_u = 650$ K using the PREMIX code of CHEMKIN [63]. The laminar flame speed, S_L, is reproduced to within a maximum difference in the laminar flame speed for both R161 and R203 with respect to D561 that is less than 2 cm/s (Fig. 9(a)). The computed flame temperatures T_f are in excellent agreement (Fig. 9(b)). The flame structure is also accurately captured as shown in Fig. 10 for the stoichiometric mixture.

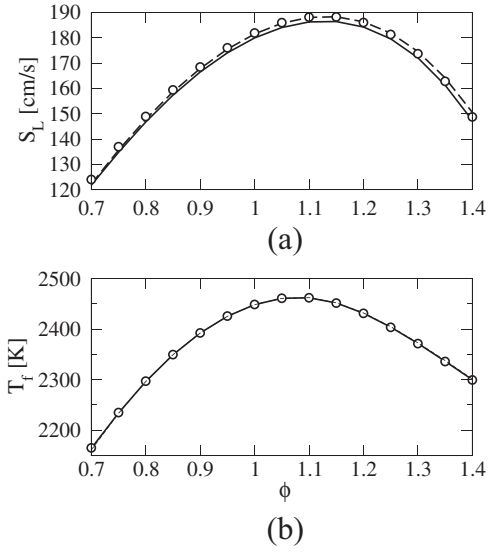

Fig. 9. (a) Laminar flame speed S_L and (b) flame temperature T_f ($p = 1$ atm, unburned mixture temperature $T_u = 650$ K; D561: solid line, R203: circles, R161: dashed line).

The computational time with the skeletal mechanisms is at least one order of magnitude lower since the significant reduction in the number of species drastically reduces the computational cost for the evaluation of the right hand side and the Jacobian.

It should be stressed that Eq. (22) describes only the contribution of the reaction to the total entropy production. However, the premixed flame application demonstrates the validity of the skeletal mechanism generated using homogeneous reactor results. In a laminar flame the total entropy generation includes not only chemical reactions but also, contribution of viscosity, heat conduction and mass diffusion. It has been shown however [64] that the major process for entropy production is entropy generation due to the chemical reactions.

5. Conclusions

In this work, we have proposed and validated the entropy production analysis for the skeletal reduction of detailed mechanisms. Important reactions are identified based on their relative contribution to the total entropy production above a user-specified threshold. Application to the detailed LLNL2 mechanism for *n*-heptane with 561 species resulted in skeletal mechanisms with 203 and 161 species. The same comprehensive mechanism has been used for skeletal reduction with different approaches. For $600 \leqslant T \leqslant 1800$ K, $1 \leqslant p \leqslant 40$ atm and $0.5 \leqslant \phi \leqslant 1.5$, 188 species by DRG, and for $700 \leqslant T \leqslant 1100$ K, $6.5 \leqslant p \leqslant 40$ atm and $0.5 \leqslant \phi \leqslant 2.0$, 177 and 185 species by CSP are available in the literature with comparable accuracy with the skeletal mechanisms found by entropy production analysis. The skeletal mechanisms exhibit good agreement not only for the homogeneous auto-igniting system, PSR and a single-zone engine model, but also for the

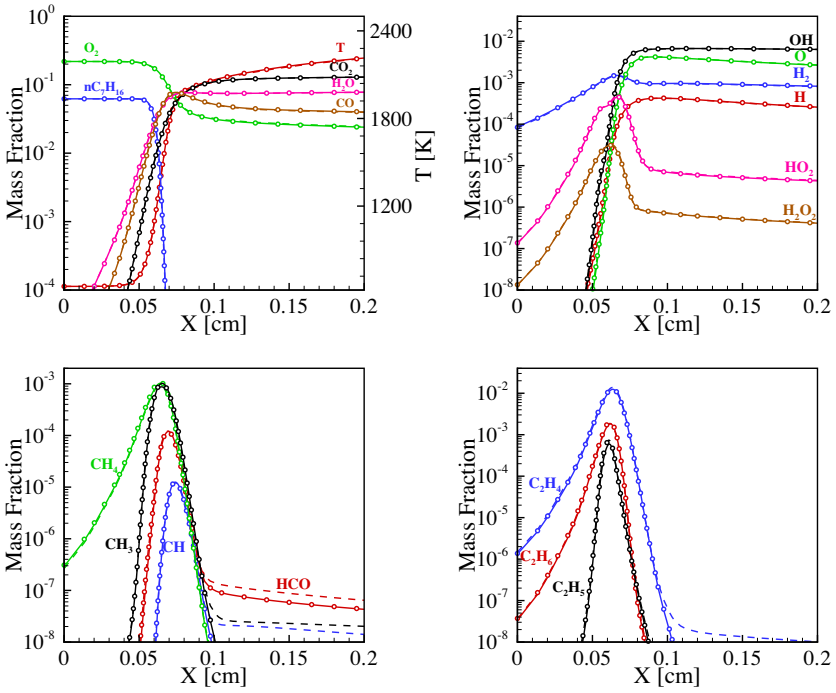

Fig. 10. Temperature and selected species profiles of the premixed laminar flame ($p = 1$ atm, $T_u = 650$ K and $\phi = 1$; D561: solid line, R203: circles, R161: dashed line).

spatially varying laminar premixed flames where diffusion of heat and species plays an important role. In addition to the lower number of species, the skeletal mechanisms are less stiff than the detailed mechanism and computational implementations show significant speedup.

The proposed approach can be easily applied on large detailed mechanisms of realistic fuels to produce skeletal schemes with promising ratio of reduction (e.g. 71% reduction for R161). Even for simpler hydrocarbon fuels like CH_4 (53 species and 256 reactions [65]), the same analysis for lean condition shows significant reduction down to 21 species and 87 reactions. For smaller detailed mechanisms (e.g. hydrogen oxidation with 9 species and 21 reactions [66]), the analysis results in schemes with smaller number of reactions but with unchanged number of species. The physical basis of the entropy production analysis and the simplicity of the algorithm warrants the investigation of its potential for the efficient adaptive (on-the-fly) chemistry reduction.

Acknowledgments

Financial support of the Swiss National Foundation under Project number 137771 is gratefully acknowledged. I.V.K. gratefully acknowledges the European Research Council (ERC) Advanced Grant 291094-ELBM.

Appendix A. Code segment for the entropy production analysis

A database 'samples.dat' is generated by the constant enthalpy and pressure batch reactor solution, using the detailed mechanism for initial conditions covering the range of interest. Pressure, p, temperature, T and mass fraction of all species Y, are stored row-wise in the file 'sample.dat'. KK and II are the number of species and reactions, respectively, and ICWRK and RCWRK the integer and real CHEMKIN work arrays. The stoichiometric matrix is stored in NUKI, forward and reverse reaction rates in the FWDK and REVK arrays, while the relative contribution of reactions to the total entropy production DSDT is stored in DSDTK. If its contribution is larger than the threshold, CUTOFF, the reaction is flagged in the array REINDX. Species participating in important reactions are flagged in array SPINDX. A slightly modified version of MECHMOD 3.42 [53] was used to generate the skeletal mechanisms by eliminating unimportant species from the detailed scheme.

```
1 OPEN (unit = 10,file='samples.dat',form='formatted')
2 100 CONTINUE
3    READ (UNIT = 10, FMT = *,END = 200) P,T, (Y (K),K = 1,KK)
4     CALL CKYTX (Y,ICKWRK,RCKWRK,X)
5     CALL CKKFKR (P,T,X,ICKWRK,RCKWRK,FWDK,REVK)
6     DO K = 1,II
7       DSDTK (K) = 0.0d0
8     ENDDO
9     DSDT = 0.d0
10    DO K = 1,II
11      IF (FWDK (K).LE.0.0d0) FWDK (K) = 1.0D-50
12      IF (REVK (K).LE.0.0d0) REVK (K) = 1.0D-50
13    DSDTK (K) = RU*(FWDK (K)-REVK (K))*(log ((FWDK (K)/REVK (K))))
14      DSDT = DSDT + DSDTK (K)
15    ENDDO
16    DO K = 1,II
17      IF ((DSDTK (K)/DSDT).gt.CUTOFF) ENT_IDX (K)=1
18    ENDDO
19      GO TO 100
20 200 CONTINUE
21    J = 0
22    DO K = 1, II
23      IF (ENT_IDX (K).eq.1) THEN
24        J = J + 1
25        REINDX (J)=K
26      ENDIF
27    ENDDO
28    CALL CKNU (KK, ICKWRK, RCKWRK, NUKI)
```

```
  DO I = 1,KK
    SPINDX (I)=0
  ENDDO

  DO K = 1, SIZEINDX
    J = REINDX (K)
    DO I = 1, KK
      IF (NUKI (I,J).ne.0) THEN
        SPINDX (I)=1
      ENDIF
    ENDDO
ENDDO
```

References

[1] D.A. Schwer, P. Lu, W.H. Green, Combust. Flame 133 (2003) 451–465.
[2] T. Lu, C.K. Law, Prog. Energy Combust. Sci. 35 (2009) 192–215.
[3] D. Goussis, U. Maas, Model Reduction for Combustion Chemistry, Fluid Mechanics and Its Applications, vol. 95, Springer, Netherlands, 2011.
[4] S.B. Pope, Proc. Combust. Inst. 34 (2013) 1–31.
[5] S. Pope, Combust. Theory Model. 1 (1997) 41–63.
[6] S.R. Tonse, N.W. Moriarty, M. Frenklach, N.J. Brown, Int. J. Chem. Kinet. 35 (2003) 438–452.
[7] H. Hiemann, D. Schmidt, U. Maas, J. Eng. Math. 31 (1997) 131–142.
[8] F.A. Williams, Combustion Theory, Addison-Wesley Pub. Co., 1965.
[9] S.H. Lam, D.A. Goussis, Proc. Combust. Inst. 22 (1989) 931–941.
[10] U. Maas, S. Pope, Combust. Flame 88 (1992) 239–264.
[11] A. Gorban, I. Karlin, Chem. Eng. Sci. 58 (2003) 4751–4768.
[12] W. Zhang, V. Kirk, J. Sneyd, M. Wechselberger, J. Math. Neuro. 1 (2011) 1–22.
[13] T. Lu, C.K. Law, Combust. Flame 144 (2006) 24–36.
[14] K. He, M.G. Ierapetritou, I.P. Androulakis, Combust. Flame 155 (2008) 585–604.
[15] A.S. Tomlin, M.J. Pilling, T. Turnyi, J.H. Merkin, J. Brindley, Combust. Flame 91 (1992) 107–130.
[16] A. Massias, D. Diamantis, E. Mastorakos, D. Goussis, Combust. Flame 117 (1999) 685–708.
[17] S. Vajda, P. Valko, T. Turnyi, Int. J. Chem. Kinet. 17 (1985) 55–81.
[18] I. Banerjee, M.G. Ierapetritou, Combust. Flame 144 (2006) 619–633.
[19] B. Bhattacharjee, D.A. Schwer, P.I. Barton, W.H. Green, Combust. Flame 135 (2003) 191–208.
[20] M. Valorani, F. Creta, D.A. Goussis, J.C. Lee, H.N. Najm, Combust. Flame 146 (2006) 29–51.
[21] T. Lu, Y. Ju, C.K. Law, Combust. Flame 126 (2001) 1445–1455.
[22] T. Lu, C.K. Law, Combust. Flame 154 (2008) 761–774.
[23] M. Valorani, F. Creta, F. Donato, H.N. Najm, D.A. Goussis, Proc. Combust. Inst. 31 (2007) 483–490.
[24] T. Lu, C.K. Law, Proc. Combust. Inst. 30 (2005) 1333–1341.
[25] T. Lu, C.K. Law, Combust. Flame 146 (2006) 472–483.
[26] T. Lu, C.K. Law, Combust. Flame 154 (2008) 153–163.
[27] Z. Luo, T. Lu, J. Liu, Combust. Flame (2011).
[28] P. Pepiot-Desjardins, H. Pitsch, Combust. Flame 154 (2008) 67–81.
[29] K.E. Niemeyer, C.-J. Sung, Combust. Flame 158 (2011) 1439–1443.
[30] X. Zheng, T. Lu, C. Law, Proc. Combust. Inst. 31 (2007) 367–375.
[31] K.E. Niemeyer, C.-J. Sung, M.P. Raju, Combust. Flame 157 (2010) 1760–1770.
[32] L. Tosatto, B. Bennett, M. Smooke, Combust. Flame 158 (2011) 820–835.
[33] C. Frouzakis, K. Boulouchos, Combust. Sci. Technol. 159 (1) (2000) 281–303.
[34] W. Sun, Z. Chen, X. Gou, Y. Ju, Combust. Flame 157 (2010) 1298–1307.
[35] H. Karadeniz, H.S. Soyhan, C. Sorusbay, Combust. Flame 159 (2012) 1467–1480.
[36] G. Li, H. Rabitz, Chem. Eng. Sci. 45 (1990) 977–1002.
[37] H. Huang, M. Fairweather, J. Griffiths, A. Tomlin, R. Brad, Proc. Combust. Inst. 30 (2005) 1309–1316.
[38] T. Lu, C.K. Law, Combust. Flame 148 (2007) 117–126.
[39] L. Liang, J.G. Stevens, J.T. Farrell, Proc. Combust. Inst. 32 (2009) 527–534.
[40] L. Liang, J.G. Stevens, S. Raman, J.T. Farrell, Combust. Flame 156 (2009) 1493–1502.
[41] F. Contino, H. Jeanmart, T. Lucchini, G. DErrico, Proc. Combust. Inst. 33 (2011) 3057–3064.
[42] J. Keck, Prog. Energy Combust. Sci. 16 (1990) 125–154.
[43] G. Beretta, J. Keck, M. Janbozorgi, H. Metghalchi, Entropy 14 (2012) 92–130.
[44] Z. Ren, S. Pope, A. Vladimirsky, J. Guckenheimer, J. Chem. Phys. 124 (2006).
[45] D. Lebiedz, J. Chem. Phys. 120 (2004) 6890.
[46] A.N. Al-Khateeb, J.M. Powers, S. Paolucci, A.J. Sommese, J.A. Diller, J.D. Hauenstein, J.D. Mengers, J. Chem. Phys. 131 (2009) 024118.
[47] V. Bykov, G. Yablonskii, T. Akramov, Doklady Akademii Nauk USSR 234 (1977) 621–634.
[48] V. Dimitrov, Simple kinetics, Nauka, Novosibirsk, 1982.
[49] I. Prigogine, Introduction to Thermodynamics of Irreversible Processes, vol. 1, Interscience, New York, 1967.
[50] A. Gorban, I. Karlin, Invariant manifolds for physical and chemical kinetics, vol. 660, Springer, 2005.
[51] T. de Donder, P. Van Rysselberghe, Thermodynamic Theory of Affinity, Stanford University Press, 1936.
[52] D. Kondepudi, I. Prigogine, Modern Thermodynamics: From Heat Engines to Dissipative Structures, Wiley, 1998.
[53] http://garfield.chem.elte.hu/Combustion/mechmod.htm.
[54] R. Kee, F. Rupley, E. Meeks, J. Miller, CHEMKIN-III: A FORTRAN Chemical Kinetics Package For the Analysis of Gas-phase Chemical and Plasma Kinetics, Sandia National Laboratories Livermore, CA, 1996.
[55] A. Gorban, E. Mirkes, G. Yablonsky, Physica A 392 (2013) 1318–1335.
[56] N. Peters, G. Paczko, R. Seiser, K. Seshadri, Combust. Flame 128 (2002) 38–59.
[57] https://www-pls.llnl.gov/?url=science_and_technology-chemistry-combustion-nc7h16, 1998.
[58] H. Curran, P. Gaffuri, W. Pitz, C. Westbrook, Combust. Flame 114 (1998) 149–177.
[59] J. Prager, H.N. Najm, M. Valorani, D.A. Goussis, Proc. Combust. Inst. 32 (2009) 509–517.
[60] L. Tosatto, B.A.V. Bennett, M.D. Smooke, Combust. Flame 160 (2013) 1572–1582.
[61] P. Brown, G. Byrne, A. Hindmarsh, SIAM J. Sci. Stat. Comp. 10 (1989) 1038–1051.
[62] J.B. Heywood, Internal Combustion Engine Fundamentals, vol. 930, McGraw-Hill, New York, 1988.
[63] R. Kee, J.F. Grcar, M. Smooke, J. Miller, Sandia report SAND85-8240, 1985.
[64] K. Nishida, T. Takagi, S. Kinoshita, Proc. Combust. Inst. 29 (2002) 869–874.
[65] G. Smith, D. Golden, M. Frenklach, N. Moriarty, B. Eiteneer, M. Goldenberg, C. Bowman, R. Hanson, S.S., W. Gardiner, V. Lissianski, Z. Qin, <http://www.me.berkeley.edu/gri_mech>.
[66] J. Li, Z. Zhao, A. Kazakov, F. Dryer, Int. J. Chem. Kinet. 36 (2004) 566–575.